DETC2007-35592

ANALYSIS AND MITIGATION OF DEAD-ZONE EFFECTS ON SYSTEMS USING TWO-IMPULSE ZV INPUT SHAPING

Khalid L. Sorensen
Woodruff School of Mechanical Engineering

Patrick W. Cross
Woodruff School of Mechanical Engineering

William E. Singhose[*]
Woodruff School of Mechanical Engineering
Georgia Institute of Technology
Atlanta, Georgia 30332
Email: Singhose@gatech.edu

Shashvat Prakash
Woodruff School of Mechanical Engineering

ABSTRACT

Input shaping is an effective method for reducing oscillatory motion in linear systems. Many physical systems, however, exhibit discontinuous dynamics, such as saturation, rate limiting, backlash, and dead-zone. These hard nonlinearities can degrade the vibration reducing properties of shaped signals. This paper investigates the detrimental effects of dead-zone on a class of input-shaped commands. A mitigation strategy is proposed for reducing these detrimental effects when the value of the dead-zone can be estimated. The robustness of this mitigation approach to uncertainties in the dead-zone width is also determined. Theoretical developments are experimentally verified using an industrial 10-ton bridge crane.

1 INTRODUCTION

Input shaping is a command filtering technique used to reduce motion-induced oscillation. It has been used to mitigate unwanted oscillation in cranes [1–4], coordinate measuring machines [5–7], satellites [8, 9], micro-milling machines [10], and long-reach manipulators [11, 12].

Input shaping is implemented by convolving a sequence of impulses, called an input shaper, with a baseline command [13, 14]. The convolution product, instead of the original baseline command, is then issued to the system. For baseline commands that reach a steady-state value, and for correctly designed input shapers, a linear system will exhibit zero residual oscillation in response to the modified command. This scenario is illustrated in Fig. 1. The original command (in this case a step) is modified by the two-impulse input shaper. Then, the shaped command actuates G. The result is zero residual oscillation.

The two-impulse input shaper used in this example is called a zero-vibration (ZV) shaper [13, 14] defined as:
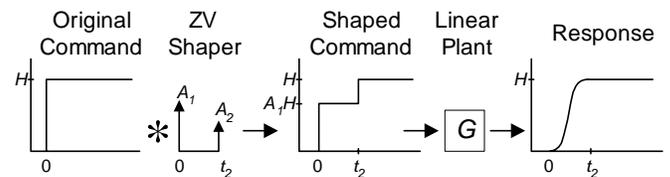

Figure 1. INPUT SHAPING PROCESS.

---

[*]Address all correspondence to this author.

$$IS(t) = A_1\delta(t) + A_2\delta(t - t_2). \tag{1}$$

The symbol $\delta(t)$ is the Dirac delta function. The input shaper parameters A_1, A_2, and t_2 are functions of ζ and ω_n, the damping ratio and natural frequency of G, respectively:

$$A_1 = \frac{e^{\pi\zeta\omega_n/\omega_d}}{1 + e^{\pi\zeta\omega_n/\omega_d}}, \tag{2}$$

$$A_2 = 1 - A_1, \tag{3}$$

$$t_2 = \frac{\pi}{\omega_n\sqrt{1-\zeta^2}} \equiv \frac{\pi}{\omega_d}. \tag{4}$$

As illustrated in Fig. 1, when a step command of magnitude H is modified by a ZV shaper, the resulting shaped command becomes a staircase command with a final magnitude of H. The ZV-shaped step command is significant because it represents a common actuating signal in input shaping applications. The oscillatory response of a plant to this command can be regarded as a performance benchmark for the ZV-shaped system in general. This is analogous to the step-response performance benchmark often used for non-input-shaped systems. For the reader interested in additional details related to input shaping theory, there are numerous references available in addition to those previously mentioned [15–19].

While input shaping works effectively for linear systems, hard nonlinearities can significantly reduce the capacity of shaped commands to eliminate oscillation [20–22]. This is because nonlinearities can corrupt input-shaped signals. This scenario is depicted in the block diagram of Fig.2(a). The *IS* block is an input shaper, and G is a linear plant. Note that rather than the shaped signal, $y_s(t)$, actuating the plant, the signal, $y_d(t)$, corrupted by the dead-zone block, actuates the plant. Figure 2(b) illustrates how a ZV-shaped step command can be corrupted by a dead-zone nonlinearity. The dead-zone element generates zero output within a region called the dead-zone. The upper and lower limits of the dead-zone are specified by $\pm d$. As the severity of the dead-zone parameter, d, increases, so does the severity of the command corruption.

The detrimental effects of dead-zone on ZV-shaped step commands have been investigated [22]. The study provided a theoretical framework for quantifying the oscillation induced into linear systems as a result of dead-zone. An inverse-dead-zone strategy for mitigating these oscillatory effects was also
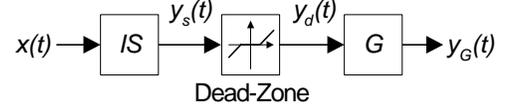
(a) Serial input shaper, dead-zone, and linear plant block diagram.
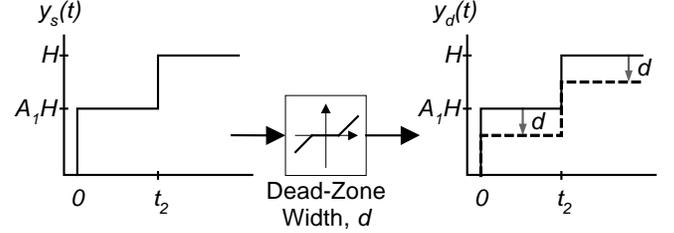
(b) ZV-shaped step command corrupted by dead-zone.

Figure 2. INPUT SHAPING IMPLEMENTED ON A SYSTEM WITH DEAD-ZONE.

proposed. However, the robustness of the mitigation technique to uncertainties in the dead-zone parameter was not considered.

The objective of the work presented here is to experimentally validate the theoretical developments presented in [22], while also investigating the robustness of the mitigation strategy to dead-zone uncertainty. To accomplish these objectives, Section 2 briefly describes an analysis technique developed in [23] by which the oscillation induced into a linear plant by arbitrary commands can be determined. This technique is used in Section 3 to predict the oscillatory effects of dead-zone on systems with ZV-shaping. Experiments performed on a 10-ton industrial bridge crane are used to verify predicted results. The inverse-mitigation technique is presented in Section 4, along with an examination of its robustness to uncertainties in the dead-zone width. Experiments from the 10-ton crane are again used to validate predicted results.

2 OSCILLATORY EFFECTS OF ARBITRARY COMMANDS ON LINEAR PLANTS

A straightforward approach to assessing the effects of various commands on a linear plant is to measure the amount of oscillation induced into the plant by the commands. By comparing the amount of oscillation caused by each command, a preference for one command over another can quickly be established.

To formalize this approach, consider the system shown in Fig. 3. G represents a damped harmonic oscillator. The finite signal $y_{np}(t)$ is an arbitrary input issued to G, conforming to the following constraints:

$$y_{np}(t) = 0, \qquad t \le 0, \tag{5}$$
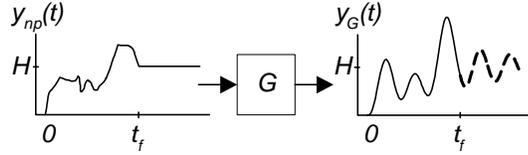
$$y_{np}(t) = H, \qquad t \ge t_f. \tag{6}$$

Figure 3. RESPONSE OF A HARMONIC OSCILLATOR TO AN ARBITRARY COMMAND.

Residual oscillation is the oscillation exhibited by a plant after the input has reached a steady-state value. The residual oscillation of G is shown with the dashed line in Fig. 3. Residual oscillation can be represented in the phase plane by a vector $\boldsymbol{R}$, defined as [23]:

$$\boldsymbol{R} = e^{-\zeta\omega_n t_f} \int_0^{t_f} \dot{y}_{np}(t) e^{t(\omega_n\zeta + \omega_d j)} dt, \qquad (7)$$

The phase of $\boldsymbol{R}$ is equal to the phase shift of the residual oscillation. The magnitude of $\boldsymbol{R}$ is proportional to the amplitude of residual oscillation at time t_f. More specifically, $|\boldsymbol{R}|$ is the ratio between two numbers, $P_{y_{np}}$ and P_{unit}. $P_{y_{np}}$ is the amplitude of residual oscillation, measured at time t_f, that would be induced into G by the signal $y_{np}(t)$. Similarly, P_{unit} is the amplitude of residual oscillation, measured at time 0, that would be induced into G by a *unit* step command. Thus,

$$|\boldsymbol{R}| = \frac{P_{y_{np}}}{P_{unit}}. \qquad (8)$$

The utility of the $\boldsymbol{R}$-value is that it may be used as an indicator of the anticipated system vibration in response to an arbitrary command. For example, suppose that a given command yields $\boldsymbol{R}$ = 10. This would indicate the the amplitude of residual oscillation exhibited by the plant in response to the command would be 10-times greater than that induced by a unit step command. An $\boldsymbol{R}$-value of zero indicates that a system exhibits no residual oscillation in response to a given command. Often, this is the most desirable scenario.

The $\boldsymbol{R}$-value can be expressed in the Laplace domain as:

$$\boldsymbol{R} = e^{-\zeta\omega_n t_f} \left[sY_{np}(s) \right]_{s=-\zeta\omega_n - j\omega_d}. \qquad (9)$$

Therefore, the magnitude of $\boldsymbol{R}$ is:

$$|\boldsymbol{R}| = e^{-\zeta\omega_n t_f} \left| sY_{np}(s) \right|_{s=-\zeta\omega_n - j\omega_d}. \qquad (10)$$

The significance of Eqns. (7),(9), and (10) is that the oscillatory effects of an arbitrary signal (limited by the aforementioned constraints) may be ascertained from either the integral of

the signal's derivative or the Laplace representation of the signal evaluated at a particular value of s.

This is a related result of an analysis conducted by Bhat and Miu in the time domain [24], and later by Park et. al. in the digital domain [25]. They demonstrated that a linear system exhibits zero residual vibration when the command signal has zeros at the system's flexible poles.

3 DETRIMENTAL EFFECTS OF DEAD-ZONE ON ZV-SHAPED STEP COMMANDS

One objective of this section is to apply the $\boldsymbol{R}$-value analysis technique to ZV-shaped step commands that have been corrupted by dead-zone. The analysis will provide an understanding of how much oscillation is caused by dead-zone in ZV-shaped systems. This analysis is presented in Section 3.1. A second objective is to validate predicted effects experimentally. However, one challenge associated with experimental verification is isolating the oscillatory effects caused by dead-zone from other non-linearities inherent to the experimental testbed. This difficulty is discussed in Sections 3.2 and 3.3 for a 10-ton industrial bridge crane with dead-zone and rate-limit nonlinearities. Finally, Section 3.4 presents experimental results from the crane.

3.1 *R*-value Analysis

Figure 2(b) previously illustrated how a ZV-shaped step command is corrupted by dead-zone. A piecewise formula for the corrupted command is:

$$y_d(t) = \begin{cases} 1(t)(A_1 H - d) + 1(t - t_2)(A_2 H), & 0 \le d < HA_1 \\ 1(t - t_2)(H - d), & HA_1 \le d < H \\ 0, & H \le d \end{cases} \qquad (11)$$

where $1(t)$ is the Heaviside function.

By forming the Laplace transform of Eqn. (11), and then substituting the result into Eqn. (10), one obtains the $\boldsymbol{R}$-value representation of the oscillatory effects of dead-zone on the ZV-shaped step command:

$$|\boldsymbol{R}| = \begin{cases} de^{-\pi\zeta/\sqrt{1-\zeta^2}}, & 0 \le d < HA_1 \\ H - d, & HA_1 \le d < H \\ 0, & H \le d \end{cases} \qquad (12)$$

Equation (12) is plotted with the solid lines in Fig. 4. The different shades of solid lines are used to indicate the cases for different damping ratios. Both the vertical and horizontal axes have been normalized to the value of H.

Because the amplitude of residual system oscillation varies directly with the magnitude of $\boldsymbol{R}$, non-zero values of the solid
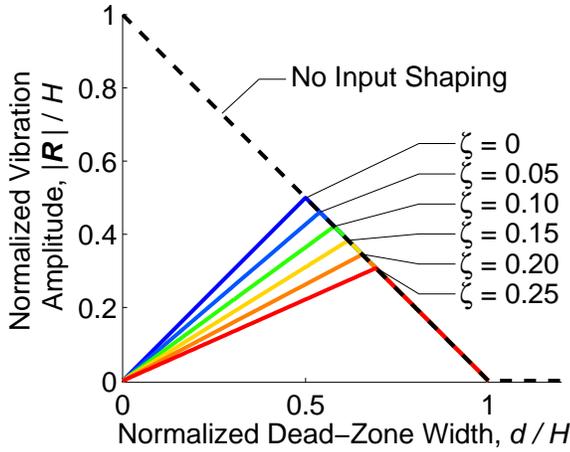
Figure 4. OSCILLATORY EFFECTS OF DEAD-ZONE ON A ZV-SHAPED AND UNSHAPED STEP COMMAND.

Figure 5. 10-TON BRIDGE CRANE.

lines indicate when the nonlinearity diminishes the vibration-reducing properties of ZV-shaped commands. The amplitude of the induced oscillation is proportional to the magnitude of R, for the given values of d and ζ. The command that excites the maximum amount of residual oscillation is produced when the system has zero damping, and the value of d is half the value of H. When the dead-zone width, d, is equal to zero, the R-value is identically zero. This observation reveals the anticipated result that in the absence of dead-zone, the harmonic oscillator will not exhibit residual oscillation in response to shaped commands. Likewise, for values of d greater than H, R is also identically zero. However, this is because the system is not actuated and remains stationary.

For the purpose of comparison, a dashed line has been added to Fig. 4. This line represents the oscillatory response caused by dead-zone when input shaping is not used. This scenario results when the *IS* block in Fig. 2(a) is reduced to unity and the input, $x(t)$, remains a step command of magnitude H.

The utility of the R-value plots shown in Fig. 4 is that they provide a concise quantitative description of the oscillatory effects of dead-zone on a harmonic oscillator. The magnitude of oscillation caused by step and ZV-shaped step commands is shown as a function of the system parameters, d and ζ. It can be seen that dead-zone degrades the inherent vibration reducing properties of ZV-shaped step commands. Additionally, the dashed line provides a baseline by which to judge the effectiveness of input shaping at reducing oscillation in the presence of dead-zone. Clearly, for values of $d < H/2$, it is predicted that the input-shaped signals induce much less oscillation than the unshaped commands.

3.2 Experimental Procedure

Figure 5 shows a photograph of a 10-ton industrial bridge crane located at the Georgia Institute of Technology (Georgia Tech). A block diagram of the crane actuation process is shown in Fig. 6. The block, *NP*, represents the nonlinear functionality of the system drives and motors. This plant accepts velocity commands issued to the crane and converts the reference velocity to the actual velocity of the overhead trolley. A programmable dead-zone width, d, is associated with this block, as well as an inherent rate-limit. The block, G, is a linear transfer function relating the velocity of the overhead trolley to the velocity of the suspended payload:

$$G = \frac{V_{payload}}{V_{trolley}} = \frac{2\zeta\omega_n s + \omega_n^2}{s^2 + 2\zeta\omega_n s + \omega_n^2}. \qquad (13)$$

This model reveals that the linear portion of the system behaves like a damped harmonic oscillator. The damping ratio is approximately 0.01.

The results of Section 3.1 predict that if ZV-shaped step commands are issued to the crane, then the dead-zone inherent to the drives and motors will degrade these commands, thus causing the payload to oscillate. A method to experimentally validate these results consists of the following four steps:

1. Issue a velocity step command of magnitude H to the system with the dead-zone parameter set to zero. Measure the magnitude of the residual payload oscillation in response to this command. This measurement is equal to $H \cdot P_{unit}$. This is illustrated in Fig. 7(a).

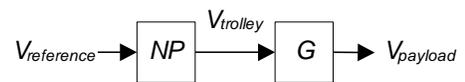2. Similarly, issue ZV-shaped velocity step commands to the

Figure 6. CRANE ACTUATION BLOCK DIAGRAM.

(a) Oscillation induced by a step command.

(b) Oscillation induced by a dead-zone affected staircase command.

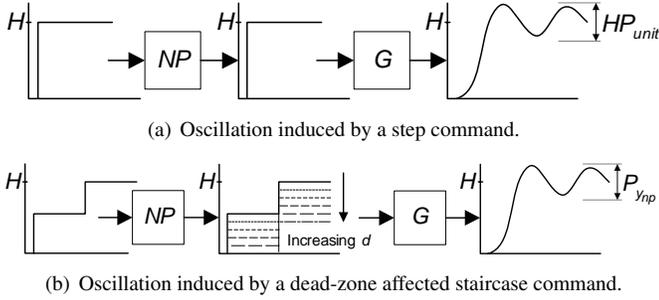Figure 7. P-VALUES FOR A SYSTEM WITH DEAD-ZONE.

system. Measure $P_{y_{np}}$ for different values of d. This is illustrated in Fig. 7(b).

3. Normalize the $P_{y_{np}}$ values obtained in Step #2 by $H \cdot P_{unit}$. The resulting ratios, $P_{y_{np}}/(H \cdot P_{unit})$, are equal to $|R|/H$ by Eqn. (8). They represent the experimentally obtained oscillatory effects of dead-zone on ZV-shaped step commands.

4. Compare the measured values of $|R|/H$ with the theoretical predictions of $|R|/H$ previously plotted in Fig. 4.

One attribute of this procedure is important to consider: physical systems are incapable of instantaneously changing velocity. Therefore, the drives and motors cannot move the trolley with the infinite acceleration commands shown in Fig. 7. Instead, velocity profiles will be issued to G that are consistent with the maximum achievable acceleration (rate-limit) of the system. This scenario is illustrated in Fig. 8. The slope of the velocity profiles is indicative of the rate-limit inherent to the drives and motors plant, NP.

Because both rate-limiting and dead-zone are present in the system, the compound effects of these nonlinearities will be exhibited in the measurements of residual oscillation. Therefore, the amplitudes P_{unit} and $P_{y_{np}}$ that would be obtained in the case that infinite acceleration were possible will be replaced with $\widehat{P}_{unit}$ and $\widehat{P}_{y_{np}}$. These amplitudes are shown in Fig. 8. A natural ques-

(a) Oscillation induced by a rate-limited step command.

(b) Oscillation induced by a dead-zone and rate-limited affected staircase command.
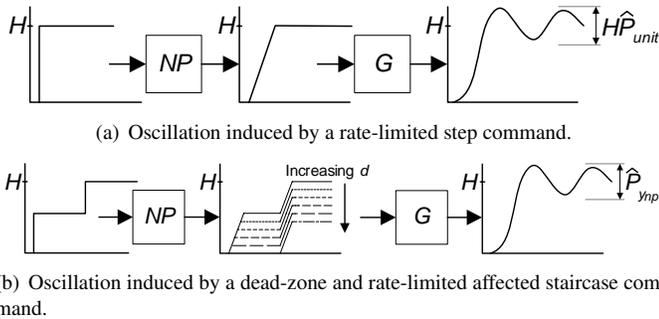
Figure 8. $\widehat{P}$-VALUES FOR A SYSTEM WITH DEAD-ZONE AND RATE-LIMITING.

tion arising from this circumstance is: *Can measurements of $\widehat{P}_{unit}$ and $\widehat{P}_{y_{np}}$ be used instead of P_{unit} and $P_{y_{np}}$ to validate the predicted effects of dead-zone?*

3.3   Isolating the Effects of Dead-Zone

To address the posed question, a ratio of $\widehat{P}$-values can be evaluated as the severity of the rate-limit is varied. The desired ratio can be obtained through an R-value analysis because of the following equality:

$$\frac{\widehat{P}_{y_{np}}}{H \cdot \widehat{P}_{unit}} = \frac{|\widehat{R}_{y_{np}}|}{|\widehat{R}_{unit}|} \tag{14}$$

$\widehat{R}_{y_{np}}$ are the R-values for the rate-limited/dead-zone signals previously shown in Fig. 8(b), and $\widehat{R}_{unit}$ are the R-values for the rate-limited step command shown in Fig. 8(a).

R-Value Analysis: The R-value for an arbitrary command, $y_{np}(t)$, acting on an undamped harmonic oscillator may be determined in the Laplace domain from:

$$|R| = |sY_{np}(s)|_{s=-j\omega}. \tag{15}$$

Applying Eqn. (15) to the rate-limited step command of Fig. 8(a) results in:

$$|\widehat{R}_{unit}| = \left| \frac{KH}{2\pi j} \left(1 - e^{2\pi j/K} \right) \right|, \quad \text{where} \tag{16}$$

$$K = \frac{T}{t_r}. \tag{17}$$

K is a non-dimensional ratio that indicates the severity of the acceleration limit. It is the ratio between the period of oscillation for the harmonic system, and the rise time of the acceleration-limited step command. A large value of K indicates that the system is capable of achieving high accelerations. A small value of K indicates that the system is sluggish.

Applying Eqn. (15) to the rate-limited, staircase commands of Fig. 8(b) results in:

$$|\widehat{R}_{y_{np}}| = \begin{cases} \left| \frac{KH}{2\pi j} \left[e^{jt_a} + e^{jt_b} \right] \right|, & 0 \le d < \frac{H}{2} \\ \left| \frac{KH}{2\pi j} \left[1 + e^{jt_c} \right] \right|, & \frac{H}{2} \le d \le H \end{cases} \tag{18}$$

5

where

$$t_a = \frac{2\pi}{K}\left(\frac{1}{2} - \frac{d}{H}\right), \tag{19}$$

$$t_b = \frac{\pi}{K}\left(1 + K\right), \qquad \text{and} \tag{20}$$

$$t_c = \frac{\pi}{K}\left(2 - 2d + K\right). \tag{21}$$

The required ratio is obtained by dividing Eqn. (18) by Eqn. (16). The result is a scalar function of the dead-zone parameter, d, and the parameter describing the severity of the rate-limit, K. The value of this ratio forms the surface shown in Fig. 9(a). Sections of the surface are shown in Fig. 9(b) for various K values ranging from $K = 2$ to $K = \infty$.

The case when $K = \infty$ is significant. This value of K results when the physical system is not restricted by a rate-limit. Thus, the line corresponding to $K = \infty$ represents the oscillatory effects of pure dead-zone on ZV-shaped step commands, without the influence of a rate-limit. Notice that for values of $K \geq 4$, the corresponding lines are nearly indistinguishable from one another. The value of K for the Georgia Tech crane is approximately 8.
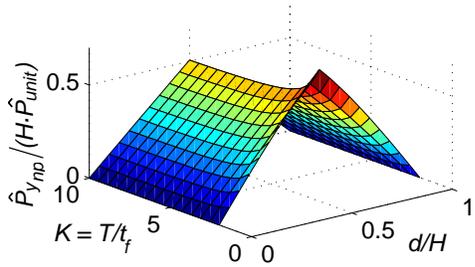
(a) Surface plot.
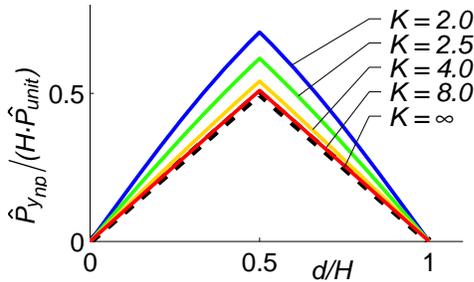
(b) Section plot.

Figure 9. OSCILLATORY EFFECTS OF ACCELERATION-LIMITED, DEAD-ZONE COMMANDS.

This result indicates that the inherent acceleration limit of the crane is negligible, and that:

$$\frac{\widehat{P}_{y_{np}}}{H \cdot \widehat{P}_{unit}} \cong \frac{P_{y_{np}}}{H \cdot P_{unit}} \equiv \frac{|\boldsymbol{R}|}{H}, \qquad \text{for } K \geq 4. \tag{22}$$

Therefore, given the light damping of the crane, the experimental procedure delineated in Section 3.2 can be used confidently to measure the oscillatory effects of dead-zone on ZV-shaped step commands.

3.4 Experimental Results

The experimental procedure of Section 3.2 was implemented with the 10-ton crane. First, a step command was issued to the crane with the dead-zone parameter set to zero. The induced motion of the suspended hook was recorded by a machine vision system, and later analyzed to obtain the residual oscillation amplitude of the motion, $H \cdot P_{unit}$. Second, a series of ZV-shaped step commands was issued to the crane, each command corresponded to a different dead-zone width. The dead-zone width was varied from $d = 0$ to $d = H$ (H being the maximum velocity of the crane). The system response for a typical trial is shown in the time plot of Fig. 10. This plot shows the commanded velocity, trolley velocity, and payload swing for the trial when d was set to 25% of the maximum velocity. The swing amplitude, $P_{y_{np}}$, corresponding to each of the d-values tested, was measured. Normalizing these values by $H \cdot P_{unit}$ resulted in the desired ratios.

The resulting ratios obtained from this experiment are plotted with the circles in Fig. 11. For comparison purposes, the theoretical results for the undamped case are also plotted. The similarity between these two results validates that 1) dead-zone reduces the effectiveness of ZV-shaped commands in a significant and predictable manner, and 2) the $\boldsymbol{R}$-value analysis technique is a reliable tool for predicting such detrimental effects.
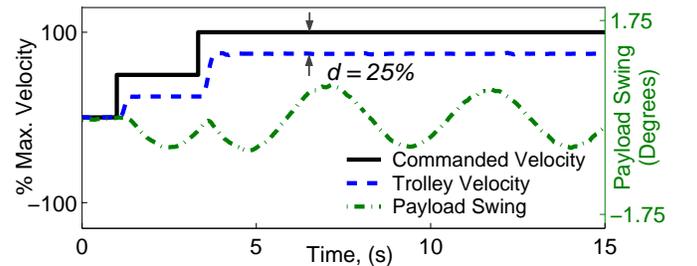

Figure 10. VELOCITY COMMAND AND SYSTEM RESPONSE FOR $d = 25\%$ MAXIMUM VELOCITY.
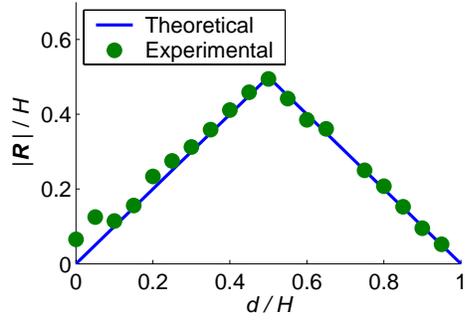
Figure 11. EXPERIMENTAL AND THEORETICAL EFFECTS OF DEAD-ZONE ON ZV-SHAPED STEP COMMANDS.

4   DEAD-ZONE MITIGATION

The functional relationship between the input and the output of dead-zone is well understood and well documented [26]. Approaches used throughout the literature to reduce the problems caused by this element utilize the dead-zone inverse function defined as:

$$Inverse(\alpha) = \alpha + \text{sign}(\alpha)d_m, \tag{23}$$

where d_m is the modeled dead-zone value of the actual dead-zone width, d.

To reduce the effects of dead-zone on an input-shaping system, an inverse-dead-zone element can be incorporated into the system in the manner depicted in Fig. 12. The response of the inverse block to shaped commands is $y_m(t)$. From this block diagram, it is apparent that if the modeled dead-zone parameter, d_m, is equal to the actual dead-zone parameter, d, then $y_d(t)$ is equal to $y_s(t)$ because the sequential dead-zone and inverse-dead-zone reduce to unity. In this scenario, the shaped signal, $y_s(t)$, acts directly on the linear plant, G, so that residual oscillation is eliminated. However, estimating the actual dead-zone width on a physical system may be difficult. Consequently, the robustness of the mitigation technique to uncertainties in the dead-zone width is considered in Section 4.1. Experimental results of the mitigation technique with uncertain dead-zone width are presented in Section 4.2.
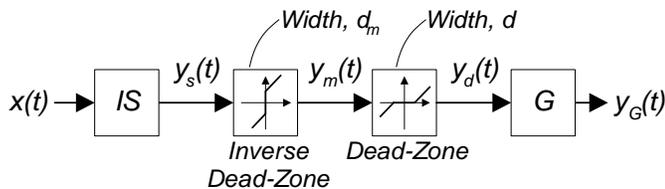

Figure 12. MITIGATION TECHNIQUE FOR ELIMINATING THE EFFECTS OF DEAD-ZONE.

4.1   Robustness to Dead-Zone Width Uncertainties

To determine the robustness of the inverse mitigation approach on ZV-shaped systems, one can consider how much oscillation is induced into a given system as a result of a specified uncertainty in the dead-zone width. To this end, consider $y_d(t)$, the signal acting directly on G. This signal is the result of a progression of command modifications to the original ZV-shaped step command, $y_s(t)$. The first modification is caused by the inverse dead-zone block to produce $y_m(t)$. This signal is further modified by the actual dead-zone to produced $y_d(t)$.

Figure 13 illustrates these modifications for different ranges of d. When d is small compared to H, the modified commands will look similar to those shown in Fig. 13(a). The solid line is the original ZV-shaped step command. This command is shifted upward by the inverse-dead-zone block by a value of d_m, resulting in the command shown with the dashed line. This command is shifted downward by the dead-zone block by a value of d, producing the command shown with the dotted line. Figure 13(b) shows a similar modification sequence, but for larger values of d.

The oscillation caused by $y_d(t)$ can be determined from an R-value analysis of this signal. Accordingly, the Laplace transform of the $y_d(t)$ signals shown in Fig. 13 can be substituted into Eqn. (10) to obtain the R-value in terms of relative uncertainty in the dead-zone width:

$$|R| = \begin{cases} \left| dEe^{-\pi\zeta/\sqrt{1-\zeta^2}} \right|, & 0 \le d < HA_1 + d_m \\ |H - dE|, & HA_1 + d_m \le d < H + d_m \\ 0, & H + d_m \le d \end{cases} \tag{24}$$

where E is the relative uncertainty between d_m and d:

$$E \equiv \frac{d_m - d}{d}. \tag{25}$$

A value of $E = 0.3$, for example, represents a 30% overestimation of the dead-zone width. A value of $E = -0.2$ represents a

(a) Case 1: $0 \le d < HA_1 + d_m$.   (b) Case 2: $HA_1 + d_m \le d < H + d_m$.
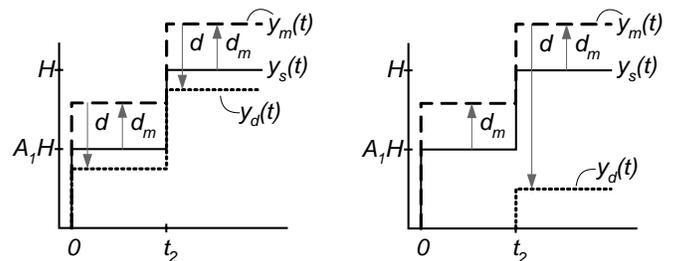
Figure 13.   ZV-SHAPED STEP COMMAND MODIFIED BY DEAD-ZONE AND INVERSE-DEAD-ZONE.

7

20% underestimation of the dead-zone width.

The R-value of $y_d(t)$ can alternatively be expressed in terms of the absolute uncertainty between d_m and d:

$$|R| = \begin{cases} 0, & -\infty < D \le -H \\ |H + D|, & -H < D \le -HA_1 \\ \left| De^{-\pi\zeta / \sqrt{1-\zeta^2}} \right|, & -HA_1 < D \le d_m \end{cases} \qquad (26)$$

where D is the absolute uncertainty between d_m and d:

$$D \equiv d_m - d. \qquad (27)$$

Equation 24 is plotted for the undamped case with the dashed lines in Fig. 14 for various values of E. Both the horizontal and vertical axis are normalized to the value of H. Nonzero values on the vertical axis are proportional to the magnitude of residual oscillation caused by $y_d(t)$. The case when the dead-zone width is overestimated ($E > 0$) is shown in Fig. 14(a).
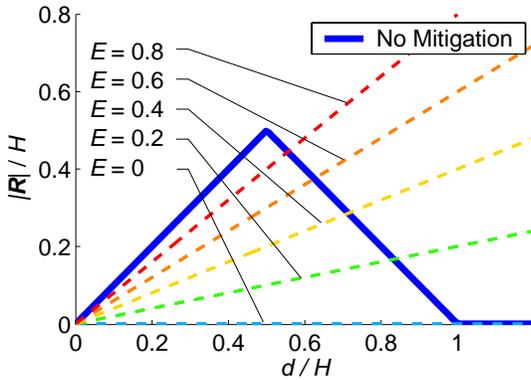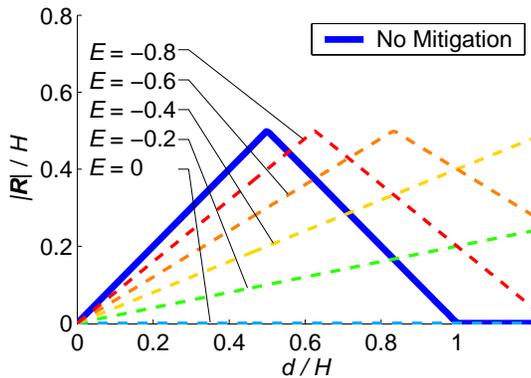
The case when the dead-zone width is underestimated ($E < 0$) is shown in Fig. 14(b).

For comparison purposes, the R-value plot for the undamped case previously shown in Fig. 4 is also plotted in Fig. 14 with the solid line. This line represents the oscillation caused by dead-zone when no mitigation is used. Thus, Fig. 14 concisely describes the robustness of the inverse-mitigation approach in terms of relative uncertainty by representing the oscillation a given dead-zone uncertainly would produce.

Notice that the line corresponding to zero relative uncertainty indicates the anticipated result that residual oscillation will be completely eliminated for all dead-zone widths. As the relative uncertainty increases, so does the anticipated oscillatory response.

A robustness graph derived in terms of absolute uncertainty is shown in Fig. 15, where Eqn. (26) is plotted for several different damping ratios. Along the horizontal axis, the absolute uncertainty, D, is varied. When D is less than zero, the dead-zone parameter, d, is underestimated. Likewise, when D is greater than zero, d is overestimated.

Both Figs. 14 and 15 provide insight into how system oscillation varies as uncertainty in the dead-zone parameter varies.

4.2 Experimental Results

The results of the robustness analysis were verified on the 10-ton Georgia Tech crane. Several known dead-zone widths, d, were manually programmed into the crane drives ranging from $d = 0$ to $d = H$. For each dead-zone width, a series of ZV-shaped step commands were issued to the crane. These commands were modified by an inverse-dead-zone function with estimated dead-zone width, d_m. The residual oscillation caused by each command was measured, then normalized by the residual oscillation amplitude caused by a velocity step command of magnitude H.

To show the measured results from this series of trials, the graphs of Fig. 14 are replotted in Fig. 16 with the addition of the experimental data. The similarity between the measured and predicted results validates the preceding robustness analysis.

(a) $E > 0$.

(b) $E < 0$.

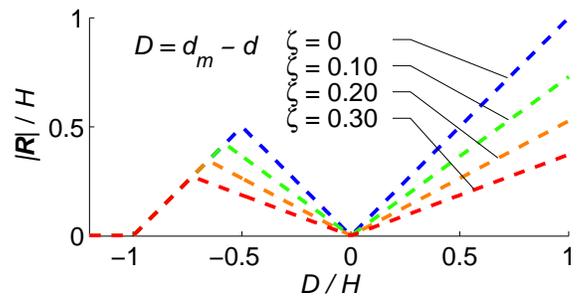Figure 14. INVERSE-MITIGATION ROBUSTNESS: RELATIVE UNCERTAINTY.

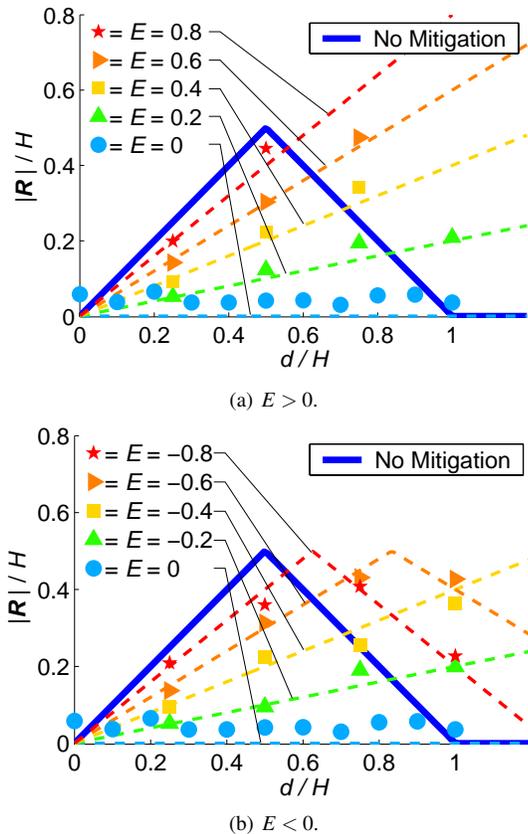Figure 15. INVERSE MITIGATION ROBUSTNESS: ABSOLUTE UNCERTAINTY.

Figure 16. EXPERIMENTAL & THEORETICAL INVERSE-MITIGATION ROBUSTNESS.

5 CONCLUSION

The detrimental effects of dead-zone on input-shaped systems are manifest in residual system oscillation. A simple relationship has been derived for quantifying the residual oscillation in terms of the dead-zone width. This relationship was used to predict the effectiveness of ZV-input shaping at eliminating oscillation in the presence of dead-zone. It was shown that dead-zone-induced oscillation on ZV-shaped systems is always less than or equal to dead-zone-induced oscillation on systems without input shaping. An inverse-dead-zone technique was proposed for mitigating the oscillatory effects of dead-zone. The robustness of the approach to uncertainties in the dead-zone width was analyzed. Experiments on a 10-ton industrial bridge crane were used to validate key results, namely 1) dead-zone deteriorates the vibration reducing properties of ZV-shaped commands in a noticable and predictable manner, and 2) inverse-mitigation of dead-zone on ZV-shaped systems can be effective even with dead-zone uncertainty.

REFERENCES

[1] Singer, N., Singhose, W., and Kriikku, E., 1997. "An input shaping controller enabling cranes to move without sway". In ANS 7th Topical Meeting on Robotics and Remote Systems.

[2] Sorensen, K., Singhose, W., and Dickerson, S., 2005. "A controller enabling precise positioning and sway reduction in cranes with on-off actuation". In IFAC World Congress.

[3] Blackburn, D. F., Singhose, W., Kitchen, J. P., Petrangenaru, V. P., Lawrence, J., Kamoi, T., and Taura, A., 2006. "Advanced input shaping algorithm for nonlinear tower crane dynamics". In 8th Int. Conf. on Motion and Vibration Control.

[4] Sorensen, K. L., Singhose, W. E., and Dickerson, S., 2007. "A controller enabling precise positioning and sway reduction in bridge and gantry cranes". *Control Engineering Practice,* **15**(July), pp. 825 – 837.

[5] Seth, N., Rattan, K., and Brandstetter, R., 1993. "Vibration control of a coordinate measuring machine". In IEEE Conf. on Control Applications, pp. 368–73.

[6] Singhose, W., Singer, N., and Seering, W., 1996. "Improving repeatability of coordinate measuring machines with shaped command signals". *Precision Engineering,* **18**(April), pp. 138–146.

[7] Jones, S., and Ulsoy, A. G., 1999. "An approach to control input shaping with application to coordinate measuring machines". *J. of Dynamics, Measurement, and Control,* **121**(June), pp. 242–247.

[8] Singhose, W. E., Porter, L. J., Tuttle, T. D., and Singer, N. C., 1997. "Vibration reduction using multi-hump input shapers". *J. of Dynamic Systems, Measurement, and Control,* **119**(June), pp. 320–326.

[9] Tuttle, T. D., and Seering, W. P., 1996. "Vibration reduction in flexible space structures using input shaping on mace: Mission results". In IFAC World Congress.

[10] Fortgang, J., Singhose, W., Marquez, J. d. J., and Perez, J., 2005. "Command shaping for micro-mills and cnc controllers". In American Control Conf., pp. 4531–4536.

[11] Love, L. J., Magee, D. P., and Book, W. J., 1994. "A comparison of joint control algorithms for teleoperated pick and place tasks using a flexible manipulator". In IEEE Int. Conf. on Systems, Man, and Cybernetics, Vol. 2, pp. 1257–62.

[12] Magee, D. P., and Book, W. J., 1995. "Filtering micromanipulator wrist commands to prevent flexible base motion". In American Control Conf., pp. 924–928.

[13] Smith, O. J. M., 1957. "Posicast control of damped oscil-

9

latory systems". *Proceedings of the IRE,* **45**(September), pp. 1249–1255.

[14] Singer, N. C., and Seering, W. P., 1990. "Preshaping command inputs to reduce system vibration". *J. of Dynamic Systems, Measurement, and Control,* **112**(March), pp. 76–82.

[15] Singhose, W., Seering, W., and Singer, N., 1994. "Residual vibration reduction using vector diagrams to generate shaped inputs". *J. of Mechanical Design,* **116**(June), pp. 654–659.

[16] Tuttle, T. D., and Seering, W. P., 1994. "A zero-placement technique for designing shaped inputs to suppress multiple-mode vibration". In American Control Conf., pp. 2533 – 2537.

[17] Singhose, W., Singer, N., and Seering, W., 1995. "Comparison of command shaping methods for reducing residual vibration". In European Control Conf., Vol. 2, pp. 1126–1131.

[18] Singhose, W. E., Seering, W. P., and Singer, N. C., 1996. "Input shaping for vibration reduction with specified insensitivity to modeling errors". In Japan-USA Symposium on Flexible Automation, Vol. 1, pp. 307–313.

[19] Huey, J. R., and Singhose, W., 2005. "Stability analysis of closed-loop input shaping control". In IFAC World Congress.

[20] Lawrence, J., Falkenberg, M., and Singhose, W., 2004. "Input shaping for a flexible, nonlinear, one-link robotic arm with backlash". In Japan-USA Symposium on Flexible Automation.

[21] Lawrence, J., Singhose, W., and Hekman, K., 2005. "Friction-compensating command shaping for vibration reduction". *J. of Vibration and Acoustics,* **127**, pp. 307–314.

[22] Sorensen, K., and Singhose, W., 2007. "Effects of common hard nonlinearities on input shaped signals". In American Control Conf.

[23] Sorensen, K. L., and Singhose, W. E., 5 Feb. 2007. "Command-induced vibration analysis using input shaping principles". *Submitted to Automatica*.

[24] Bhat, S. P., and Miu, D. K., 1990. "Precise point-to-point positioning control of flexible structures". *J. of Dynamic Systems, Measurement, and Control,* **112**(4), pp. 667–674.

[25] Park, U., Lee, J., Lim, B., and Sung, Y., 2001. "Design and sensitivity analysis of an input shaping filter in the z-plane". *J. of Sound and Vibration,* **243**(1), pp. 157–171.

[26] Tao, G., and Kokotovic, P. V., 1995. "Continuous-time adaptive control of systems with unknown backlash". *IEEE Trans. on Automatic Control,* **40**(6).